Inner shell excitation spectroscopy of transient molecules: HBS, HBO, and $H_3B_3O_3$

L. E. Ennis and A. P. Hitchcock
Department of Chemistry, McMaster University, Hamilton, Ontario, Canada L8S 4Ml

(Received 16 April 1999; accepted 2 June 1999)

Inner shell electron energy spectroscopy (ISEELS) was used to study HBS, HBO, and $H_3B_3O_3$, reactive, transient species generated *in situ*. The reaction of H_2S with crystalline boron in a quartz tube was used to produce thioborine (HBS) at ~1100 °C, and borine (HBO) at ~1200 °C. The reaction of H_2O vapor with crystalline boron in a quartz tube at ~1200 °C was used to produce boroxine ($H_3B_3O_3$). These species were identified from their inner shell excitation spectra and mass spectrometry. The B 1*s*, S 2*s*, and S 2*p* ISEEL spectra of HBS, and the B 1*s* and O 1*s* spectra of HBO and $H_3B_3O_3$ are reported and analyzed with the help of GSCF3 *ab initio* calculations. A reaction scheme is proposed for the generation of HBO from the reaction of H_2S and boron in a heated quartz tube. © *1999 American Institute of Physics.* [S0021-9606(99)01632-3]

I. INTRODUCTION

The spectroscopy of transient species and reactive intermediates is of interest both to identify novel chemical species and to understand reaction mechanisms.[1] Various methods of generating and detecting short-lived species have been coupled to a wide variety of spectroscopic techniques. Mass spectrometry can be used to detect and confirm the presence of intermediates; microwave and infrared spectroscopies provide quantitative structural information; photoelectron spectroscopy investigates the occupied electronic structure; UV-visible optical spectroscopy can provide both geometric and structural information.[2] In this work we report the first systematic application of inner shell electron energy loss spectroscopy (ISEELS) to the detection and characterization of reactive transient species.

Inner-shell excitation spectra, recorded using either x-ray absorption[3] or inelastic electron scattering (ISEELS),[4] have been used for many years to investigate the electronic structure of stable gas phase atoms and molecules.[5] In ISEELS, a quasimonoenergetic beam of high-energy electrons is used to excite an electron in a core orbital of the system under study, and the kinetic energy spectrum of the inelastically scattered electrons is measured. The energy lost by the incident electron beam corresponds to a specific core excitation event. The technique can be applied over wide energy ranges (50–1500 eV in the gas phase) so that element specific core excitation spectra can be recorded for most elements in the Periodic Table. At high impact energy and small scattering angle, ISEEL spectra are dominated by electric-dipole allowed transitions. With appropriate corrections, such spectra can be converted to their optical counterpart with an absolute oscillator strength (or cross section) scale.[5] With the apparatus used for this study, ISEEL spectra can be recorded from any species for which a vapor pressure of at least 1×10^{-6} Torr can be achieved.

ISEELS offers several advantages for the detection and study of transients and reaction intermediates. The technique is very sensitive and thus it is readily coupled to a wide variety of transient generation techniques. Core excitation is element specific and thus wide scans provide a rapid and very helpful monitor of the elemental composition of the sample under study. Even in molecules with several chemical sites for the same element, spectral features of specific chemical environments can often be identified. The spectral contribution from a single core edge is readily converted to an absolute intensity scale using normalization of the continuum intensity to atomic values.[5] Establishing absolute intensity scales is very helpful in unraveling the spectra of mixtures and also in confirming species identification by comparison of both intensity and energy patterns to calculated spectra. As this paper illustrates, inner shell spectroscopy can be used for direct chemical identification.

In order to demonstrate the utility of inner shell spectroscopy for the detection and identification of transient species, we have studied the products of the heterogeneous reaction of $H_2S(g)$ at the surface of solid boron. This system was chosen since numerous studies have shown it to be an effective method of producing HBS.[6–18] In the course of our study we rather surprisingly found a new spectral signature at high temperatures, corresponding to a species containing boron and oxygen but no sulfur, which we tentatively identified as HBO.[19–34] In order to confirm our identification of this species we also studied the products of the reaction of $H_2O(g)$ at the surface of solid boron, which is known to produce boroxine, $H_3B_3O_3$.[19,20] Comparison of the B 1*s* and O 1*s* spectra of the species generated from the ''hot H_2S/B'' reaction with those of boroxine ruled out boroxine as the oxygen containing product. Instead, mass spectrometry and comparison to *ab initio* calculations of the core excitation spectra of HBS, HBO, $H_3B_3O_3$, $H_2B_2O_3$, and $H_3B_3O_4$ identify the

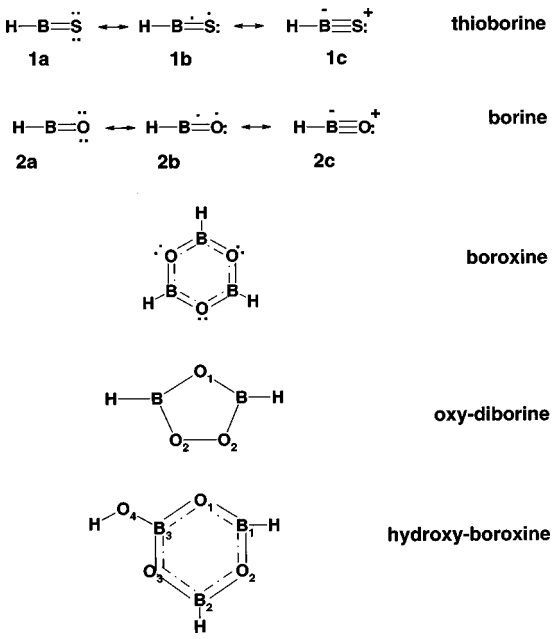

Scheme 1. Species whose core spectra were studied in this work. The more important Lewis ''resonance'' structure for HBS and HBO are indicated.

product of the ''hot H_2S/B'' reaction as HBO. Scheme 1 depicts the structures of all species investigated in this work, either experimentally or by quantum computations. We propose reaction schemes for all transient generating reactions, including that producing HBO.

A. Previous studies of thioborine (HBS), borine (HBO), and boroxine ($H_3B_3O_3$)

Kirk and Timms first observed thioborine (HBS) in 1967 using time-of-flight mass spectrometry.[6] This reactive and thus transient species was produced in the reaction of H_2S and boron at ~1100 °C under low pressure. The half life was reported to be one minute at room temperature at 0.2 mm pressure before it decayed irreversibly on the walls of the container to form polymeric $(HBS)_x$.[6] The HBS polymerization reaction was studied by Gropen and Wisløff-Nilssen,[7] who consider it to occur by attack of a H^- ion. The H_2S/B method of producing HBS has been used with many types of spectroscopy to probe its structure and properties. The rotational spectrum of HBS, recorded in 1973 by Pearson and McCormick,[8] showed that the molecule is linear in its ground state. The photoelectron spectrum of HBS was reported by Kroto *et al.*[9] and Fehlner *et al.*[10] in 1973, while Sams and Maki[11] reported the infrared spectrum in 1974. In 1993, Mebel *et al.*[12] studied the microwave spectrum of HBS generated by the pyrolysis of BH_2SH and reported the H–B and B–S bond lengths to be 1.176(1) Å and 1.605 (1) Å, respectively.

Ab initio calculations of the ground state properties of HBS have also been performed by many groups.[13–18] Thioborine, which is a linear, 10 valence electron species, was the first species known to have B–S multiple bonding.[8] The *ab initio* study of Nguyen *et al.*[15] concluded that the B–S bond in HBS is a triple bond consisting of two covalent bonds and one dative π-bond (cf. structure 1a in scheme 1). Later Talaty *et al.*[16] calculated the bond order of the B–S bond in HBS to be 2.5 (structure 1b). In 1988, calculations by Suffolk *et al.*[18] also predicted a triple bond in HBS.

HBO is much less stable than HBS. It was first reported in 1963 by Sholette and Porter[19] who observed it using mass spectrometry as an intermediate in the production of its trimer, boroxine ($H_3B_3O_3$), from the reaction of H_2O with boron. Many attempts at isolating HBO have confirmed that boroxine is much more stable than HBO.[6,9] HBO has been produced by photolysis of $H_2B_2O_3$, trapped in a low-temperature argon matrix, then detected by matrix infrared spectroscopy by Lory and Porter[20] in 1971. Transient HBO has also been generated by oxidation of B_2H_6 with N_2O or O_2.[21,22] The half life of HBO was estimated to be less than 100 ms.[21] The structure of HBO has been determined using electronic spectroscopy,[21] microwave spectroscopy,[22] and infrared spectroscopy.[23] The H–B and B–O bond lengths in HBO are 1.168(1) Å and 1.200(1) Å, respectively.[22]

Many *ab initio* studies have been performed on HBO.[15–18,24–33] As with the B–S bond in HBS, there is debate as to the nature of the B–O bond in HBO. Thomson and Wishart[24] proposed that the B–O bond is a double bond. However, the SCF study of Nguyen *et al.*[15] claimed that the B–O bond was triple and dative like the B–S bond in HBS (structure 2a). This was supported in 1991 by Talaty *et al.*[16] who described the structure as similar to HBS, and determined the B–O bond order to be 2.45 (structure 2b). One might expect HBS to have a larger bond order than HBO since S is a better π-electron donor than O, thus the B–S bond has more triple-dative bonding character.

Boroxine, $H_3B_3O_3$, is the most stable form of the HBO polymer. It has been well documented spectroscopically.[33,34] From gas phase electron diffraction[33] it is known that the trimer has a six-membered ring structure with B–O and B–H bond lengths of 1.376(2) Å and 1.19(2) Å, and B–O–B and O–B–O bond angles of 120.0(6)° (structure 3). Partial B═O double-bonding character is expected since boroxine is an analog of benzene.

II. EXPERIMENT

A. Generation of transient species

Thioborine, HBS, was generated by passing H_2S gas over a layer of crystalline boron in a quartz tube. The flow of H_2S gas (Matheson, 99.5%) was adjusted to increase the pressure in the main spectrometer vacuum chamber from a base of $\sim 1\times10^{-7}$ to between 5×10^{-7} and 6×10^{-6} Torr. The crystalline boron (Alfa Aesar, 99.5%) was ground with a mortar and pestle to increase surface area and reduce the relative amount of oxidized boron surface (the same results were found without grinding). A 6 mm diam, 45 cm long quartz tube was surrounded by an electric furnace. One end of the quartz tube was introduced directly into the spectrometer to within ~4 mm of the gas cell, while the other end was connected to a copper tube through which the H_2S was introduced from behind a leak valve. The furnace was resistively heated to raise the temperature of the quartz tube to between 1000 °C and 1200 °C, as measured by a thermocouple placed adjacent to the quartz tube at the center of the

furnace (caution must be taken not to heat the quartz tube beyond its softening temperature). Boroxine, $H_3B_3O_3$, was generated using the same experimental design but using a flow of H_2O vapor over the crystalline boron. The H_2O was distilled and purified by three ''freeze–pump–thaw'' cycles. No attempt was made to trap any of the products, although in both reactions copious amounts of colored solids were deposited on the inside of the quartz tube and on the interior walls of the spectrometer, which required frequent and extensive cleaning to maintain operability. After the ''hot H_2S/B'' reaction the portion of the quartz tube that was in the hot zone of the furnace was visibly etched.

B. Spectral acquisition

Core excitation spectra were measured with an electron energy loss spectrometer[4] using an unmonochromated electron beam operated with final electron energy of 2500 eV, ~2° scattering angle, ~0.7 eV energy resolution, and incident beam currents of up to 30 μA. Currents of ~4 μA were used to reduce space charge beam broadening and thus to acquire slightly higher energy resolution spectra (~0.5 eV FWHM) of the discrete structures. Signal averaged spectra were collected for 1–6 h. The energy scale was calibrated relative to standard lines of well known reference gases[35] (see tables). The spectra were background subtracted and the isolated core edge signal was then converted to an absolute oscillator strength scale using a conversion procedure described elsewhere.[5]

A systematic measurement of the pressure and temperature dependence of the signal intensity was performed for each reactive species studied. For each of eight temperatures between 800 and 1250 °C, B 1*s* spectra were collected at six pressures between 5×10^{-7} and 5×10^{-6} Torr at a current of 20 μA. The background was removed from each spectrum, then the areas under the strong B 1*s* peaks were measured to generate the signal intensity plots presented later. Note that the spectral changes were reversible and that they occurred virtually instantaneously with changes in the temperature of the furnace. The proposed species identification was supported by mass spectra measured with a quadrupole mass spectrometer attached to the ISEEL spectrometer, but considerably removed from line-of-sight of the collision cell. Mass spectra were collected with and without gas, at cold and hot temperatures.

C. Computational methodology

In order to gain insight into the electronic structure of the transients, calculations were performed using Gaussian self-consistent field version 3 (GSCF3),[36,37] which is an *ab initio* code designed specifically for inner shell excitation and ionization calculations. The program uses the Hartree–Fock-SCF approach to solve for the energies and molecular orbitals of the system under investigation. The basis sets used are those of Huzinaga *et al.*[38] The improved virtual orbital (IVO) method,[39] which explicitly takes into account the core hole in the Hartree–Fock approximation, is used to perform quantum calculations on core-excited molecules. In this approach, the core electron is removed directly from an inner shell orbital specified by the user. The virtual orbitals of this system provide a good approximation to the term values of the core excitation features at that site.[39] A separate calculation is performed for each distinct chemical site in each molecule (see scheme 1 for atom numbering for species with the same element in multiple environments).

TABLE I. Geometries and basis sets used for the GSCF3 Calculations of HBS, HBO, and $H_3B_3O_3$.

Species	Bond	Bond lengths (Å) and angles Distance	Bond	Angle
HBS[a]	H–B	1.169	H–B–S	180.0
	B–S	1.599		
HBO[b]	H–B	1.166	H–B–O	180.0
	B–O	1.201		
$H_3B_3O_3$[c]	H–B	1.19	O–B–O	120.0
	B–O	1.376	B–O–B	120.0
$H_2B_2O_3$[d]	B–H	1.182	B–O–B	104.0
	$B–O_1$	1.380	O–B–O	103.1
	$B–O_2$	1.365	B–O–O	105.0
	O–O	1.470	$H–B–O_1$	126.3
$H_3B_3O_4$[e]	$O_1–B_1$	1.359	$O_1–B_1–H$	120.6
	$B_1–H$	1.182	$H–B_1–O_2$	120.2
	$B_1–O_2$	1.367	$B_1–O_2–B_2$	121.1
	$O_2–B_2$	1.363	$O_2–B_2–O_3$	119.1
	$B_2–H$	1.182	$B_2–O_3–B_3$	120.7
	$B_2–O_3$	1.363	$O_3–B_3–O_1$	119.1
	$O_3–B_3$	1.375	$O_3–B_3–O_4$	121.1
	$B_3–O_1$	1.366	$B_3–O_4–H$	113.4
	$B_3–O_4$	1.340		
	$O_4–H$	0.943		

[a]From Ref. 8. Basis functions [Huzinaga *et al.* (Ref. 38)]: 3 for H, 33/3 for B, 333/33 for S. On the atom given the core hole, a larger basis function was used: 63/5 for B, 533/53 for S.
[b]From Ref. 22. Basis functions (Ref. 38): 3 for H, 33/3 for B, 33/3 for O. On the atom given the core hole, a larger basis function was used: 63/5 for B and O.
[c]From Ref. 33. Basis functions (Ref. 38): 3 for H, 33/3 for B, 33/3 for O. On the atom given the core hole, a larger basis function was used: 63/5 for B and O.
[d]From Ref. 45. Basis functions (Ref. 38): 3 for H, 33/3 for B, 33/3 for O. On the atom given the core hole, a larger basis function was used: 63/5 for B and O. See scheme 1 for labeling of oxygen atoms.
[e]Calculated using 4-31 G optimization. Basis functions (Ref. 38): 3 for H, 33/3 for B, 33/3 for O. On the atom given the core hole, a larger basis function was used: 63/5 for B and O. See scheme 1 for labeling of atoms.

Table I lists the geometries of the molecules studied, all except $H_3B_3O_4$ taken from experiment,[8,22,33,45] and the basis sets employed. The calculation is performed in three steps. In step one, the eigenvectors (MOs) and eigenvalues of the ground state are calculated, and the core MO that will lose the electron is determined. In the second step, the core ion state is computed by removing the user-specified core electron and allowing the system to relax and reorganize in the presence of the core hole. The difference in the total energy of the core-ionized and ground state gives the core level ionization potential (IP) with a typical accuracy of 1 eV. The third step determines the core excitation energies and transition probabilities in terms of the IVO approximation.[37] The absolute accuracy of the computed core excitation energies depends on the size of the basis set used. However, the core state term values ($TV=IP-E$) are more accurate and relatively independent of basis set choices. The core excitation

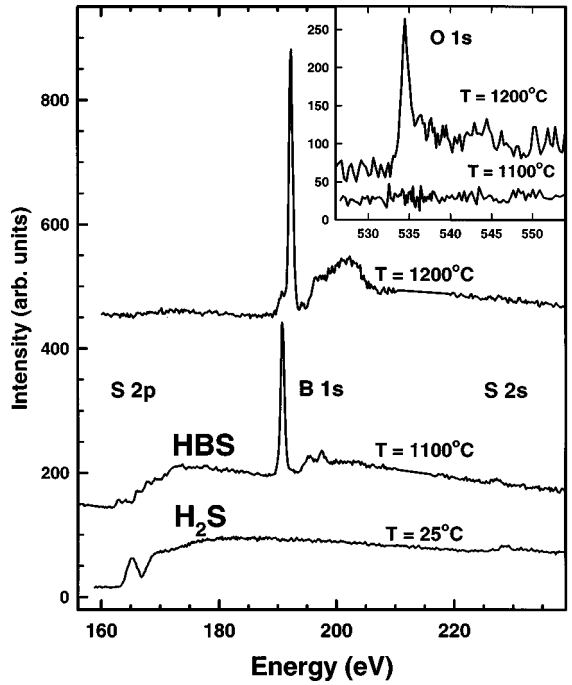

FIG. 1. Inner shell electron energy loss spectra in the S $2p$, B $1s$, and S $2s$ regions of H_2S, and the products of passing H_2S over hot boron crystals. The spectra were recorded using 2.5 keV final electron energy, 2° scattering angle, and 0.7 eV FWHM resolution. The pressure and temperature under which the middle and upper curves were obtained were (1×10^{-6} Torr, 1100 °C) and (5×10^{-6} Torr, 1200 °C), respectively. Offsets of 100 and 420 have been used. The insert plots the O $1s$ region recorded under conditions similar to those used in the middle and upper curve of the main plot.

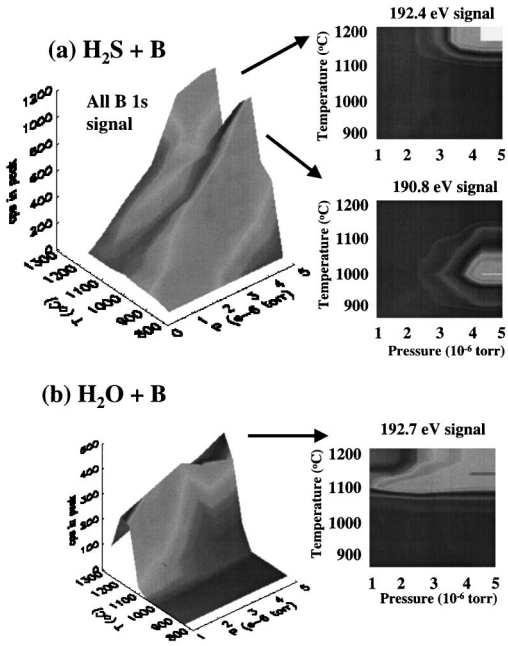

FIG. 2. (a) Strength of the B $1s$ signal from the H_2S/B reaction as a function of pressure and temperature (P,T). The 2D contour plots indicate the (P,T) distribution of the intensity of the 190.8 eV and 192.4 eV signals, while the 3D plot summarizes the (P,T) dependence of the overall B $1s$ signal. (b) Strength of the B $1s$ signal from the H_2O/B reaction, in 3D and 2D representations.

term values and optical oscillator strengths generated by the third step of the GSCF3 calculation are used to generate simulated core excitation spectra by summing Gaussian lines at an energy given by (IP-term value), an area given by the oscillator strength for excitation to each improved virtual orbital, and a width chosen as a function of the term value. In the discrete region, the chosen line width is that of the instrument while larger line widths are used for the lifetime broadened continuum resonances. The widths used are summarized in footnotes to the tables which summarize the computational results.

III. RESULTS

A. Reactions of boron with H_2S and H_2O

Representative spectra acquired as H_2S was passed over the crystalline boron in the heated quartz tube are presented in Fig. 1. These ISEEL spectra were collected in the B $1s$, S $2s$, S $2p$, and O $1s$ regions at ($P=2\times10^{-6}$ Torr, $T=25$ °C), at ($P=1\times10^{-6}$ Torr, $T=1100$ °C), and at ($P=5\times10^{-6}$ Torr, $T=1200$ °C). Below 900 °C, there was no B $1s$ or O $1s$ signal and the S $2s$ and S $2p$ spectra were those of H_2S.[40] At approximately 1000 °C, the S $2p$ and S $2s$ signal changed shape and a sharp, intense B $1s$ peak appeared at 190.8(1) eV. As the temperature was further increased to 1150 °C or higher, the 190.8 eV peak decreased in intensity, the S $2p$ and S $2s$ signal intensity dropped dramatically, and a second peak developed in the B $1s$ spectrum at 192.4(1) eV. By 1200 °C, all S $2p$ and S $2s$ features disappeared, the 190.8 eV peak became negligible, and the 192.4 eV peak dominated the entire spectrum. Simultaneously, above 1150 °C a sharp feature appeared in the O $1s$ region of the spectrum, as illustrated in the insert to Fig. 1. The pressure and temperature dependence of the B $1s$ signals at 190.8 and 192.4 eV are presented in Fig. 2(a). There is a remarkably clean differentiation of the conditions giving rise to HBS from those giving the high temperature boron oxide species, indicating a threshold for some process is exceeded in the reaction.

Given the presence of boron and oxygen and the absence of sulfur, the most likely candidates for the high temperature species are either borine (HBO) or boroxine ($H_3B_3O_3$). The very sharp, intense low energy B $1s$ and O $1s$ signals are more consistent with the ~2.5 bond order of HBO, than with the 1.5 bond order of $H_3B_3O_3$. However, previous studies of this reaction[6,9] have not reported HBO or indeed, any oxygen containing species. (Kroto *et al.*[9] actually noted changes in the photoelectron spectrum at temperatures above 1150 °C but concluded the unidentified species involved did not contain either sulfur or oxygen.) In addition, it is well known that boroxine is significantly more stable than the HBO monomer. In order to determine if the product of the ''hot H_2S/B'' reaction is boroxine, we used ISEELS to study the reaction of H_2O with hot boron, under conditions known to produce $H_3B_3O_3$. At 1150 °C strong signals were observed in the B $1s$ and O $1s$ spectra, as illustrated in Fig. 3. The shapes of these signals are different from those observed in the ''hot H_2S/B'' reaction. Careful calibration of the sharp B $1s$ peaks placed that from the H_2O/B reaction at 192.7(1) eV, 0.3 eV higher than the peak observed at 192.4(1) eV in

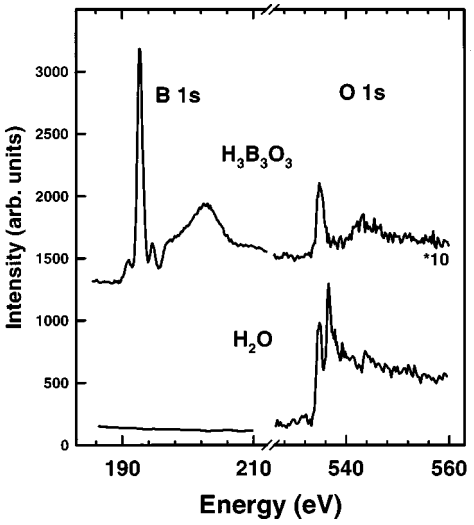

FIG. 3. ISEELS spectra in the B 1*s* and O 1*s* region from H_2O and the product of passing H_2O over boron at 1150 °C. The upper data was recorded at (5×10^{-6} Torr, 1150 °C). Offsets are used for clarity. See caption to Fig. 1 for experimental details.

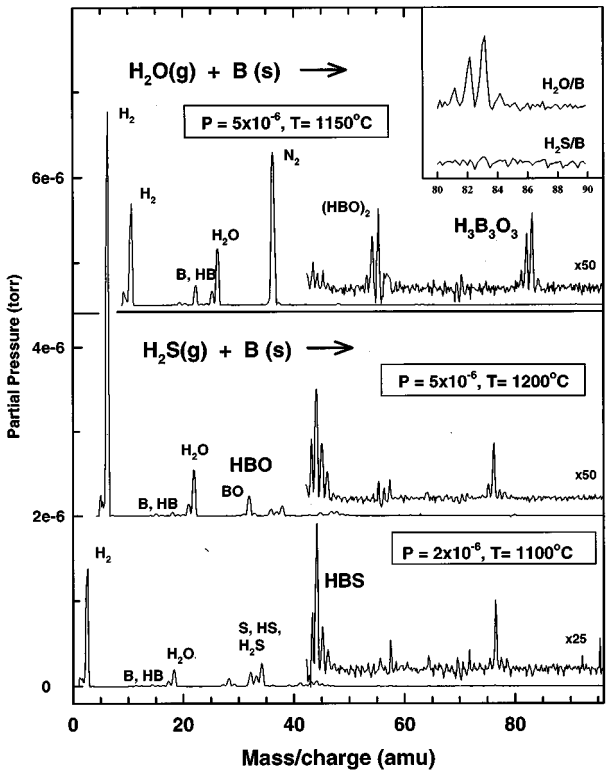

FIG. 4. Mass spectra recorded under the indicated reaction conditions. Horizontal and vertical displacements are used to avoid overlap. The signal from the no-sample background recorded just prior to heating the furnace has been subtracted.

the high temperature regime of the H_2S/B reaction. Since $H_3B_3O_3$ is known to be produced under these conditions, the main features of the spectrum from the H_2O/B reaction are assigned to $H_3B_3O_3$ (as discussed below, we suspect the weak feature at 194.6 eV and possibly that at 191.0 eV are from other boron species). The pressure and temperature dependence of the B 1*s* signal from the H_2O/B reaction is plotted in Fig. 2(b). It is distinctly different than that for the high temperature H_2S/B signal [Fig. 2(a)].

Support for our species identification is provided by *in situ* mass spectrometry. Figure 4 compares mass spectra collected during the low and high temperature H_2S/B reaction conditions and during the H_2O/B reaction. There is a strong $m/z=2$ (H_2^+) signal in the mass spectra under all reaction conditions, but it is especially strong in the hot H_2S/B reaction. Hydrogen is a by-product in the formation of both HBS and HBO (Refs. 9,10) and in the decomposition of H_2S at high temperatures. The spectrum from the H_2O/B reaction exhibits peaks at $m/z=82$ and 83, which are consistent with $H_2B_3O_3^+$ and $H_3B_3O_3^+$.[19] These peaks are absent in the hot H_2S spectrum (see insert to Fig. 4). This rules out attribution of the high temperature H_2S/B species as boroxine, and indirectly supports its attribution to HBO. Indeed in the HBS experiment, there are no high mass peaks in the mass spectrum from either the 1100 °C or 1200 °C reaction with H_2S that are consistent with the presence of $H_3B_3O_3$. The high mass signal in the H_2S experiment at $m/z\sim74$ could be due to $(HBS)_2^+$ associated with $(HBS)_x$ prepolymer species, which have been documented in other studies.[6–8]

In the mass spectra from the H_2S experiment, there is a decrease in the $m/z=32$ (S^+), 33 (HS^+), and 34 (H_2S^+) intensities, and an increase in the $m/z=27$ (BO^+), $m/z=28$ (HBO^+), and $m/z=2$ (H_2^+ intensities as the temperature is increased from 1100 °C to 1200 °C. These features are consistent with HBO production and decomposition of H_2S at higher temperatures. The fragmentation pattern in the $m/z=27-29$ region of the 1200 °C mass spectrum is consistent with the expected isotope distribution of ($^{10}BO-^{11}BO/H^{10}BO-H^{11}BO$). Weak signals at these same m/z are seen in the mass spectrum of the 1100 °C reaction, indicating some of the hot H_2S/B product was also being formed even under these conditions. Similarly, there is residual HBS signal under the higher temperature reaction conditions. The mass spectrum of the hot H_2S/B reaction is a more ambiguous signature of HBO than that detected by the ISEELS experiment. This is not surprising since the mass spectrometer is about 20 cm away from the collision cell and can only be reached by multiple wall collisions, in which the reactive HBO species would be expected to adsorb and react, leading to differential depletion of HBO relative to minority species in the reaction mixture. Note also that the H_2O^+ signal, $m/z=18$, increases under the ''hot H_2S/B'' reaction conditions, consistent with reaction of hydrogen and oxygen. Based on both the mass spectrometry and the ISEELS, we assert that the H_2S/B reaction product is HBO.

B. B 1*s* spectroscopy of HBS, HBO, and $H_3B_3O_3$

Figure 5 displays the B 1*s* oscillator strength spectra of HBS, HBO, and $H_3B_3O_3$, as well as the B 1*s* spectra of HBS, HBO, $H_3B_3O_3$, $H_2B_2O_3$, and $H_3B_3O_4$ predicted by the GSCF3 calculations. The latter two boron oxide species have been detected in small amounts in reactions between boron and oxygen.[11,46] Thus the B 1*s* spectra of $H_2B_2O_3$ and $H_3B_3O_4$ (structures 4 and 5) were computed in order to consider the possibility that the ''hot H_2S/B'' reaction product is

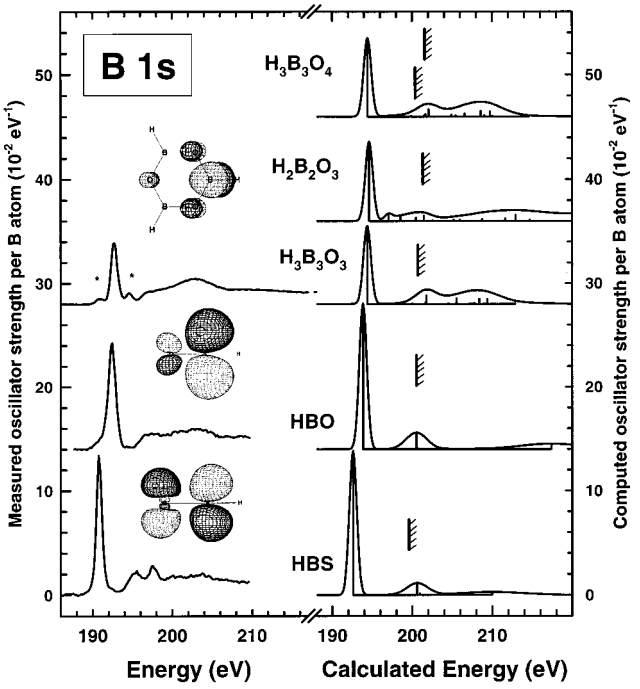

FIG. 5. (Left) Experimental B 1*s* oscillator strength spectra of the three transient species observed in this work. A background generated by extrapolation of the pre-edge signal, has been subtracted in each case. Offsets are used for clarity. The asterisks indicate peaks believed to come from species other than $H_3B_3O_3$. The computed π^* LUMO for B 1*s* core excited HBS, HBO, and $H_3B_3O_3$ are plotted. (Right) B 1*s* spectra of the indicated species computed by GSCF3. The hatched lines indicate the calculated location of the B 1*s* IP.

one of these oxides, and also to help assign small additional features in the spectrum of $H_3B_3O_3$. The predicted B 1*s* spectra for HBS, HBO, and $H_3B_3O_3$ are in generally good agreement with the spectra from the ''cool H_2S/B,'' ''hot H_2S/B,'' and the H_2O/B reactions, respectively. The predicted spectra for $H_2B_2O_3$ and $H_3B_3O_4$ are also significantly different in shape from the spectrum of the ''hot H_2S/B'' reaction product, although quite similar to the predicted B 1*s* spectrum of boroxine. Thus, comparison to computation provides further support for our interpretation of the chemistry.

The experimental B 1*s* peak energies are summarized in Table II while the main B 1*s* computational results are summarized in Table III. The lowest energy peak in all three spectra is attributed to B 1*s* excitation to the LUMO, of π^* character in all three species. Contour plots of the LUMO π^* orbital in the $(B\,1s^{-1},\pi^*)$ excited states are presented in Fig. 5. (Note that in boroxine the use of a localized core hole concentrates electron density on the core excited B atom. A linear combination of similar functions with the core hole on each B atom would be a more accurate representation.) The B 1*s*$\rightarrow\pi^*$ peak for HBS occurs at lower energy than in either HBO or $H_3B_3O_3$ because sulfur is less electronegative and thus the B 1*s* core level is less tightly bound, and also because sulfur is a better π-donor than oxygen. The latter makes the separation of the π HOMO and π^* LUMO energy levels smaller so that less energy is required for the B 1*s* $\rightarrow\pi^*$ excitation. The GSCF3 computation supports this viewpoint since the predicted B 1*s*$\rightarrow\pi^*$ energies for HBO and $H_3B_3O_3$ are higher than those for HBS. The calculated B 1*s* ionization potentials (IP's) also follow this trend, with predicted IP's of 199.5 eV, 200.3 eV, and 200.6 eV for HBS, HBO, and $H_3B_3O_3$, respectively. In addition, the sharp, intense nature of the π^* peak in HBS is consistent with the triple bonding character in the molecule.

Similarly, the B 1*s*$\rightarrow\pi^*$ excitation energy is slightly lower for HBO than for $H_3B_3O_3$ because each boron in $H_3B_3O_3$ is bound to two oxygen atoms, stabilizing the B 1*s* core level and shifting its excitation and ionization energies to higher energy. The greater intensity of the B 1*s*$\rightarrow\pi^*$ peak of HBO relative to that of $H_3B_3O_3$ found both experimentally and computationally, is consistent with the larger boron–oxygen bond order of HBO.

The calculated spectra support these interpretations. In particular they predict the same energy ordering and relative intensities for the B 1*s*$\rightarrow\pi^*$ transitions, although, as found in other applications of this GSCF3 methodology, the absolute calculated energies are about 2 eV higher than the experimental values. The overall pattern of the higher energy structures is also reproduced, although not as precisely as the energies and intensities of the strong π^* peaks. The similarity of the appearance of the calculated spectra of $H_2B_2O_3$ and $H_3B_3O_4$ to that of $H_3B_3O_3$ shows that these could be minority species in the reaction and may contribute to the spectra collected. The relative positions of the computed π^* peaks suggest that the small feature at 194.6 eV in the B 1*s* spectrum of the H_2O/B reaction may be due to one of these minority species.

TABLE II. Energies and proposed assignments for features in the B 1*s* spectra of HBS, HBO, and $H_3B_3O_3$ ($\pm$0.1 eV).

	Species			Assignment		
Peak	HBS	HBO	$H_3B_3O_3$	HBS	HBO	$H_3B_3O_3$
1′			(191.0)			···
1	190.8[a]	192.4[a]	192.7[a]	π^*	π^*	$\pi^*(a_1,b_2)$
2′			(194.6)			$\pi^*(H_3B_3O_4)$?
2	195.4	197.4(2)	197.1(2)	σ^*_{BS}	Ryd	$\pi^*(b_2)$
3	197.6	200.8(3)		Ryd	$2e$	
4	200.6(4)	203	202.9(4)		σ^*_{BO}	σ^*_{BO}
5	203.4(6)		209			

[a]Calibration: HBS +6.3(1) eV relative to the t_{2g} peak of SF_6 at 184.54(5) (Ref. 35); HBO+7.9(1) eV relative to SF_6; $H_3B_3O_3$ +8.2(1) eV relative to SF_6.

C. O 1*s* spectroscopy of HBO and $H_3B_3O_3$

The O 1*s* ISEEL spectra provide further evidence for attributing the ''hot H_2S/B'' reaction product to HBO. Figure 6 compares the O 1*s* spectra from the hot H_2S/B and H_2O/B reactions to the GSCF3 computed O 1*s* spectra of HBO and $H_3B_3O_3$. The calculated O 1*s* spectra for $H_2B_2O_3$ and $H_3B_3O_4$ are also included, and all chemically distinct oxygen sites have been considered. Relative to the B 1*s* spectra, it is clear from both the experimental and computed spectra displayed in Fig. 6 that O 1*s* is more sensitive than B 1*s* spectroscopy to chemical bonding in these boron oxide species. The energies and proposed assignments of the O 1*s* spectral features are summarized in Table IV while the energies of

TABLE III. GSCF3 computed energies (eV) for B 1*s* excited states of HBS, HB, $H_3B_3O_3$, $H_2B_2O_3$, and $H_3B_3O_4$.[a]

(A) HBS, HBO, $H_3B_3O_3$

HBS			HBO			$H_3B_3O_3$		
ϵ[b]	f[c]	Assign.[d]	ϵ[b]	f[c]	Assign.[d]	ϵ[b]	f[c]	Assign.[d]
−6.93	8.12	π^*	−6.44	8.23	π^*	−6.19	8.82	π^*
						−0.57	0.23	π^*
199.5		IP	200.3		IP	200.6		IP
1.05	1.59	π^*	0.22	2.35	π^*	1.11	0.46	π^*
1.43	0.40	σ^*_{B-S}	1.20	0.82	σ^*	1.21	2.61	σ^*_{B-O}
10.47	2.68	σ^*	0.38	0.37	σ^*_{B-O}	4.02	0.23	σ^*
			5.23	0.11	σ^*	4.97	2.82	π^*

(B) $H_2B_2O_3$, $H_3B_3O_4$

$H_2B_2O_3$			$H_3B_3O_4$ B 1*s* (O–B–O)			$H_3B_3O_4$ B 1*s* (B–OH)		
ϵ[b]	f[c]	Assign.[d]	ϵ[b]	f[c]	Assign.[d]	ϵ[b]	f[c]	Assign.[d]
−6.71	8.92	π^*	−5.72	8.78	π^*	−5.03	8.62	π^*
−4.27	0.58	π^*	−2.60	0.23	π^*	−1.06	0.35	π^*
−3.43	0.09	σ^*	−0.32	0.24	σ^*			
−2.80	1.15	σ^*	−0.30	0.16	π^*			
−0.87	1.02	σ^*						
201.3		IP	200.1		IP	201.6		IP
0.10	1.57	π^*	1.36	0.44	σ^*	1.08	1.72	π^*
1.23	0.13	σ^*	1.53	0.71	σ^*	1.08	0.13	σ^*
3.86	0.34	σ^*	1.91	2.25	π^*	2.56	0.11	σ^*
4.61	0.63	σ^*_{B-O}	4.76	0.93	σ^*	3.90	2.38	σ^*
7.41	1.07	σ^*	5.29	0.65	σ^*_{B-O}	4.78	0.89	σ^*_{B-O}
10.32	2.43	σ^*	6.40	1.56	σ^*	6.87	0.35	σ^*
11.60	5.57	σ^*	8.41	2.85	σ^*	8.00	2.27	σ^*
13.36	1.06	σ^*	8.90	0.72	σ^*	8.98	1.56	σ^*
			9.61	2.60	σ^*	9.90	1.74	σ^*

[a]Widths of Gaussian peaks used in the simulated spectra are set according to the term value (ϵ, energy of transition relative to the IP), with 1.1 eV for $-10<\epsilon<-4$ eV; 3.0 eV for $-4<\epsilon<4$ eV; 5.0 eV for $4<\epsilon<10$ eV; 12.0 eV for $10<\epsilon<25$; 15 eV for $\epsilon>25$ eV.
[b]IVO orbital energy which approximates the term value for the core excited state. The GSCF3 prediction of the absolute transition energy is IP+ϵ.
[c]Oscillator strength ($\times 10^2$) for the indicated transition.
[d]Dominant orbital character.

the computed spectral features are summarized in Table V. As with the B 1*s* spectra, the good agreement of the experimental O 1*s* spectra with those computed for HBO and $H_3B_3O_3$, as well as distinct differences from the computed O 1*s* spectra of $H_2B_2O_3$ and $H_3B_3O_4$, support our species attributions.

The intense low energy feature in each spectrum is attributed to the O $1s\rightarrow\pi^*$ transition. Contour plots of the LUMO π^* orbital in the $(O\,1s^{-1},\pi^*)$ excited states of HBO and $H_3B_3O_3$ are presented in Fig. 6 (Note that in boroxine the use of a localized core hole concentrates all density on the core excited O atom. A linear combination of similar functions with the core hole on each O atom would be a more accurate representation.) The peak in HBO occurs 0.6 eV lower in energy than that for $H_3B_3O_3$, a shift similar to that in the B $1s\rightarrow\pi^*$ transition energies. While qualitatively one might expect the O 1*s* IP to shift opposite from the B 1*s* IP, in fact the calculations predict that the O 1*s* IP of HBO is 0.9 eV lower than that of $H_3B_3O_3$. Similar to the B 1*s* spectra, the intensity of the O $1s\rightarrow\pi^*$ peak is much greater for HBO than for $H_3B_3O_3$, which is consistent with the greater boron–oxygen bond order of HBO. These trends are also found in the calculated O 1*s* spectra, although the shift in the O $1s\rightarrow\pi^*$ transition between HBO and $H_3B_3O_3$ seems exaggerated. The calculated absolute peak energies and absolute intensities for the O 1*s* spectra are very close to those found in the measured spectra, particularly for $H_3B_3O_3$.

D. S 2*s* and 2*p* spectroscopy of HBS

The S 2*p* and S 2*s* ISEEL spectra of HBS are plotted in Fig. 7 in comparison to those of H_2S, along with the GSCF3 predicted spectrum of HBS. The energies for the S 2*p* and 2*s* spectral features of H_2S and HBS are summarized in Table VI while the computed S 2*s* energies are summarized in Table VII. The S 2*p* spectrum of H_2S shows a low energy feature due to S 2*p* excitation to a low-lying σ^*_{H-S} dissociative state. This feature is absent in the S 2*p* spectrum of HBS since HBS does not have a low-lying dissociative state.[40] There is a weak, low energy contribution to the S 2*p* spectrum of HBS which we attribute to S $2p\rightarrow\pi^*$ transitions. Since the π^* orbital in HBS is mainly of S 3*p* character, this transition is weak due to poor dipole overlap.

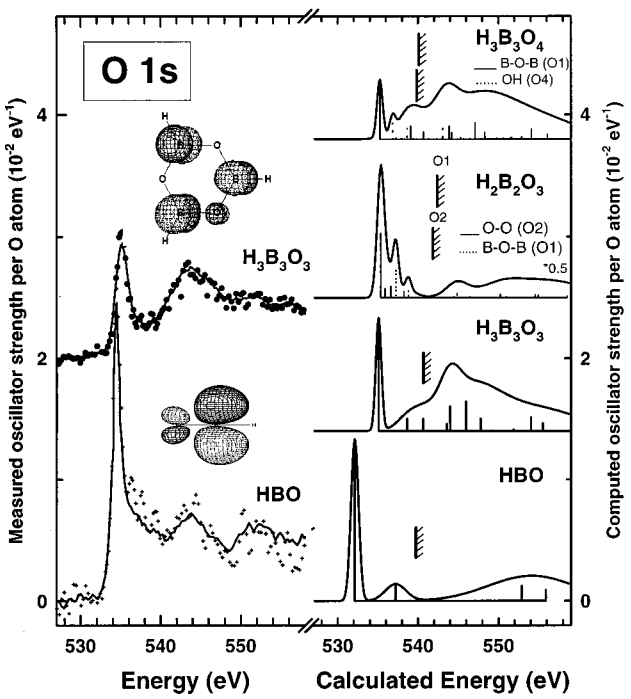

FIG. 6. (Left) Experimental O 1*s* oscillator strength spectra of the two oxygen containing transient species observed in this work. Pre-edge background has been subtracted in each case. The line is a smoothed version of the data to guide the eye. Offsets are used for clarity. The computed π^* LUMO for O 1*s* core excited HBO and $H_3B_3O_3$ are plotted. (Right) O 1*s* spectra of HBO, $H_3B_3O_3$, $H_2B_2O_3$, and $H_3B_3O_4$ computed by GSCF3. The hatched lines indicate the calculated location of the O 1*s* IP(*s*).

The S 2*s* spectrum of HBS was also examined. In general, S 2*s* spectra can be more informative about bonding than S 2*p* spectra since they sample the *p* density of states in the unoccupied levels, whereas the S 2*p* spectrum samples *s* and *d* character, which are much less important in bonding. However, the unfavorable signal to background ratio for S 2*s* spectra makes this a challenging measurement. (The S 1*s* spectrum would be much more sensitive but, at 2460 eV, it is above the energy losses accessible by ISEELS.) The lowest energy peak in the H_2S spectrum is due to the S $2s \rightarrow \sigma^*$ transition. In HBS, the lowest energy peak is assigned to the S $2s \rightarrow \pi^*$ transition which occurs at lower energy than the S $2s \rightarrow \sigma^*$ transition in H_2S since the π^* orbital in HBS is lower in energy. The S $2s \rightarrow \pi^*$ transition is quite prominent relative to the S 2*s* continuum of HBS, consistent with the strong multiple bond. The broad peak at 235 eV is attributed to S $2s \rightarrow \sigma^*_{B-S}$ transitions. The line shape and intensity of the

TABLE IV. Energies and proposed assignments for features in the O 1*s* spectra of HBO and $H_3B_3O_3$ (± 0.1 eV).

	Species		Assignment	
Peak	HBO	$H_3B_3O_3$	HBO	$H_3B_3O_3$
1	534.6[a]	535.2[a]	π^*	$\pi^*(b_2)$
2	544	544.5	σ^*_{BO}	σ^*_{BO}
3	552	552		

[a]Calibration, HBO +3.8(1) eV relative to O_2: 530.8(1) eV (Ref. 35); $H_3B_3O_3$ +4.4(1) eV relative to O_2.

reaction scheme 1

$$H_2S(g) + B(s) \longrightarrow HBS(g) + 1/2H_2(g)$$

reaction scheme 2

$$H_2S(g) \longrightarrow H_2(g) + S(s)$$
$$SiO_2(s) \longrightarrow SiO(s) + 1/2O_2(g)$$
$$B(s) + 1/2O_2(g) \longrightarrow BO(s)$$
$$BO(s) + 1/2H_2(g) \longrightarrow HBO(g)$$
$$B(s) + SiO_2(s) + H_2S(g) \longrightarrow S(s) + Si(s) + 1/2H_2(g) + 1/2O_2(g) + HBO(g)$$

reaction scheme 3

$$H_2O(g) + B(s) \longrightarrow HBO(ads) + 1/2H_2(g)$$
$$3HBO(ads) \longrightarrow H_3B_3O_3(g)$$
$$3\,H_2O(g) + 3\,B(s) \longrightarrow 3/2H_2(g) + H_3B_3O_3(g)$$

Scheme 2. Proposed reaction sequences for producing (1) HBS, (2) HBO, and (3) $H_3B_3O_3$. All reactions involving reactant or intermediate B species are considered to take place at the surface of polycrystalline boron.

GSCF3 computed signal are close to experiment, though the predicted energies are about 4 eV higher. The agreement between computed and observed S 2*p* spectral shape provides further support for our assignment of the hot H_2S/B reaction product as HBO.

IV. DISCUSSION: PROPOSED REACTION SCHEMES

Proposed reaction schemes to generate each of HBS, HBO, and $H_3B_3O_3$ are presented in Scheme 2. The Gibbs free energy for each overall reaction, calculated from the standard state Gibbs energy of formation of the reactants and products,[41] corrected for temperature and pressure, are -248 kJ/mol at 1400 K for HBS; -331 kJ/mol at 1500 K for HBO; and -384 kJ/mol at 1500 K for $H_3B_3O_3$. Thus each reaction scheme indicated in Scheme 2 is thermodynamically allowed.

HBS is generated from the reaction of H_2S and hot crystalline boron at temperatures of approximately 1100 °C, as outlined in reaction scheme 1. At higher temperatures [>1200 °C (Ref. 42)] H_2S decomposes into its constituent elements. This is evidenced in the mass spectra in Fig. 4 by the appearance of signals at m/z 2 (H_2^+) and the decrease in intensity of peaks at m/z 32 (S^+), 33 (HS^+), and 34 (H_2S^+) at higher temperatures. The high temperature decomposition of H_2S has also been documented in previous studies of the HBS reaction.[9] Presumably the onset of this decomposition abruptly terminates the reaction pathway leading to HBS. In the same temperature regime, a new pathway opens up, that leading to the species we have identified spectroscopically as HBO.

The interesting question is, where does the oxygen come from? The oxygen needed to form HBO must come from the quartz tube since there was no oxygen species present in the vapor phase (as detected by ISEELS or mass spectrometry) until the tube was heated to 1200 °C in the presence of H_2S. The observation of strong etching of the quartz tube is also

TABLE V. GSCF3 computed energies (eV) for O 1*s* excited states of HBO, $H_3B_3O_3$, $H_2B_2O_3$, and $H_3B_3O_4$.[a]

(A) HBO, $H_3B_3O_3$

HBO			$H_3B_3O_3$		
ϵ[b]	f[c]	Assign.[d]	ϵ	f	Assign.[d]
−7.60	1.56	π^*	−5.23	0.79	π^*
−2.53	0.88	σ^*_{B-O}	−1.97	0.32	π^*
539.7		IP	540.6		IP
			0.04	0.32	π^*
8.73	0.01	σ^*	2.99	0.19	σ^*_{B-O}
13.15	1.56	π^*	3.41	0.65	σ^*
			5.37	2.09	σ^*
			7.18	0.86	σ^*

(B) $H_2B_2O_3$, $H_3B_3O_4$

$H_2B_2O_3$						$H_3B_3O_4$					
O_1[e]			O_2[e]			O_1[e]			O_4[e]		
ϵ[b]	f[c]	Assign.[d]	ϵ	f	Assign.[d]	ϵ	f	Assign.[d]	ϵ	f	Assign.[d]
−7.30	1.12	π^*	−6.67	2.82	σ^*	−3.16	0.40	π^*	−4.92	0.50	π^*
−5.43	1.88	σ^*	−6.12	0.40	π^*	−1.35	1.11	π^*	−1.07	0.45	π^*
−3.87	0.52	π^*	−5.41	0.50	σ^*_{B-O}	3.07	1.49	σ^*	0.53	0.25	π^*
2.20	1.80	σ^*	−3.79	0.73	σ^*	5.33	0.35	σ^*	3.72	0.45	σ^*_{B-O}
542.6		IP	542.0		IP	540.1		IP	539.9		IP
11.49	1.47	π^*	2.44	0.20	σ^*	8.42	0.83	σ^*	4.04	0.68	σ^*
12.28	1.60	σ^*	4.40	0.11	σ^*	10.60	0.70	σ^*	5.17	0.15	σ^*
12.68	0.68	σ^*	8.24	0.62	σ^*	10.80	0.14	σ^*	6.97	1.70	σ^*
17.14	0.68	σ^*	9.00	0.18	σ^*	11.70	1.52	π^*	8.16	0.70	σ^*
			12.56	1.54	π^*	12.06	0.35	σ^*	9.65	0.09	σ^*
			12.91	1.26	σ^*	12.33	0.42	σ^*	10.45	0.04	σ^*
									11.35	0.21	σ^*

[a]Widths of Gaussian peaks used in the simulated spectra are set according to the term value (ϵ, energy of transition relative to the IP), with 0.8 eV for $-10<\epsilon<-2$ eV; 3.0 eV for $-2<\epsilon<4$ eV; 8.0 eV for $4<\epsilon<10$ eV; 12.0 eV for $\epsilon>10$ eV.

[b]IVO orbital energy which approximates the term value for the core excited state. The absolute transition energy is IP+ϵ.

[c]Oscillator strength ($\times 10^2$) for the indicated transition.

[d]Dominant orbital character.

[e]The identity of the inequivalent atoms is indicated in Scheme 1.

consistent with quartz decomposition to yield oxygen. We stress that when boron is heated to 1200 °C in a quartz tube without H_2S, this etching does not occur, there is no H_2O^+ signal beyond that in the background gas, and there are no volatile products detectable by ISEELS. In the absence of H_2S, temperatures of 2000 °C or more are required to strip oxygen from quartz.[43] However the thermodynamic threshold temperature for SiO_2 decomposition drastically decreases when a reducing agent such as H_2S is present.[43] Under H_2S flow conditions, O_2 could be present at relatively low pressures due to the H_2S-induced decomposition of the quartz. The oxygen species active in generating HBO could be either atomic or molecular, with the important species being that present on the boron surface.

It is also essential to have a source of hydrogen for the reaction to occur. This is provided by the thermal decomposition of H_2S into S and H_2 above 1150 °C. Indeed, the thermal cracking of sulfur and the concomitant trapping of elemental sulfur on the quartz or boron surface is an essential part of the explanation of our observations, since when HBO is observed there is essentially no sulfur containing species present in the vapor phase products of the reaction (see Fig. 1).

The sequence proposed to lead to HBO is outlined in reaction scheme 2. It likely includes the reaction of crystalline boron with O_2 at high temperatures to form BO.[44] A computational study by Page in 1989 (Ref. 25) claims that BO can react with H_2 to form HBO. The kinetics of this reaction were investigated in 1991 by Garland *et al.*,[45] where the BO was generated by the laser photolysis of $BCl_2(OCH_3)$. Thus we propose that HBO is formed at the boron surface by reaction with oxygen from the H_2S induced SiO_2 decomposition reaction and hydrogen from H_2S decomposition.[46]

Why doesn't boroxine form instead of HBO? Relative to the H_2O/B reaction, there is less oxygen available at the surface of the boron crystals to participate in the reaction, thus fewer HBO transients are produced. This may be an important factor in avoiding conversion to the more stable $H_3B_3O_3$. The HBO is stable long enough to be detected spectroscopically under our conditions. The estimated transit time from furnace to gas cell is estimated from kinetic theory to be ~0.5 ms. *The strategy of using oxygen generated by reductive decomposition of quartz as a means to generate less stable suboxides* appears to be remarkably successful since there was no evidence for $H_3B_3O_3$ either in the ISEEL spectra or the mass spectra.

The production of $H_3B_3O_3$ by the reaction of H_2O with

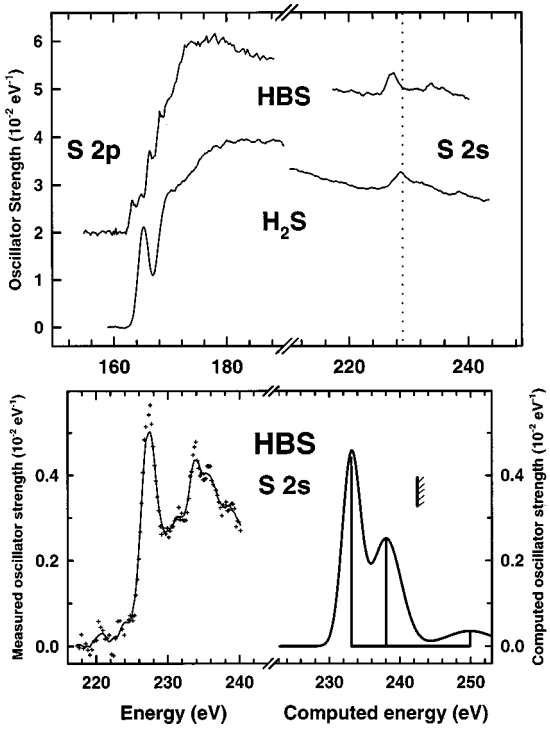

FIG. 7. (Upper) Experimental S $2s$ and S $2p$ oscillator strength spectra of HBS and H_2S. Offsets are used for clarity. (Lower) Comparison of the experimental S $2s$ signal of HBS to that computed by GSCF3. The hatched line indicates the calculated location of the S $2s$ IP.

crystalline boron (reaction scheme 3) occurs because there is a continuous flow of H_2O over the boron. Since there is more oxygen available to react at the surfaces of the boron crystals, more HBO can be produced. This in turn quickly reacts to form the more stable species, $H_3B_3O_3$. The reaction most likely occurs on the boron surface since the rate of intermolecular collisions at 10^{-6} Torr is negligible and because HBO was not detected in the ISEELS or in the mass spectrum.

TABLE VI. Energies and proposed assignments for features in the S $2p$ and S $2s$ spectra of H_2S and HBS (± 0.1 eV).

	Species		Assignment		
S $2p$			H_2S	HBS	
Peak	H_2S	HBS	$2p_{3/2}/2p_{1/2}$	$2p_{3/2}$	$2p_{1/2}$
1	165.3[a]	163.4[a]	$\sigma^*(a_1)$	π^*	
2		164.8			π^*
3		166.3		σ^*	
4	170.3(2)	168.3(2)	$\sigma^*(b_2)$		σ^*
5		169.3(3)			
6	185.5(4)	178(1)			

	Species		Assignment	
S $2s$				
Peak	H_2S	HBS	H_2S	HBS
1	228.8(2)	227.4	$\sigma^*(a_1)$	π^*
2	231.4(3)	231.2	$\sigma^*(b_2)$	σ^*_{BS}
3		234		

[a]Calibration, H_2S $-19.2(1)$ eV relative to SF_6 184.54(5) (Ref. 35); HBS $-21.1(1)$ eV relative to SF_6.

TABLE VII. GSCF3 computed energies (eV) for S $2s$ excited states of HBS.[a]

ϵ[b]	f[c]	Assignment[d]
-9.29	0.70	π^*
-4.37	1.34	σ^*_{BS}
242.4		IP
7.49	0.30	σ^*

[a]Widths of Gaussian peaks used in the simulated spectra are set according to the term value (ϵ, energy of transition relative to the IP, with 1.5 eV for $-10<\epsilon<-2$ eV; 3.0 eV, for $-2<\epsilon<4$ eV; 8.0 eV for $4<\epsilon<10$ eV; 12.0 eV for $\epsilon>10$ eV. The greater discrete width is associated with Coster–Kronig broadening of S $2s$ states.
[b]IVO orbital energy which approximates the term value for the core excited state. The absolute transition energy is IP$+\epsilon$.
[c]Oscillator strength ($\times 10^2$) for the indicated transition.
[d]Dominant orbital character.

V. SUMMARY

Inner-shell electron energy loss spectroscopy was used to investigate the spectroscopy and electronic structure of transient species. The unstable transient species, HBS was generated by reaction of H_2S and crystalline boron at 1100 °C in a quartz tube. Similarly, boroxine, $H_3B_3O_3$ was formed in the reaction between H_2O and crystalline boron at 1200 °C. At temperatures above 1150 °C in the H_2S/B reaction a new species was observed, which the evidence strongly suggests is HBO.

This work has demonstrated the usefulness of ISEELS for studying unstable molecules, in the exploration of novel chemistry, and potentially for the detection of reaction intermediates. The qualitative and semiquantitative elemental analysis provided by ISEELS, the insight offered by *ab initio* calculations, and the confirmation of species identification by mass spectrometry, is a powerful combination that can be used to investigate many different gas phase reactions as well as vapor phase products of heterogeneous chemistry.

ACKNOWLEDGMENTS

Financial support for this research was provided by NSERC. The authors thank Dr. N.P.C. Westwood for advice on the reaction chemistry; Dr. Tyliszczak and Bob Lessard for their assistance with ISEELS, and for providing continuing improvements to the spectrometer; Jim Garrett for constructing the furnace used in the experiments and for providing the boron crystals; Dr. S.G. Urquhart and J.F. Lehmann for help with calculating the geometry of $H_3B_3O_3$ and the GSCF3 procedures; and Professor N. Kosugi for generously allowing us to use his GSCF3 code.

[1] E. Hirota, *High Resolution Spectroscopy of Transient Molecules* (Springer, New York, 1985).
[2] J. M. Dyke, J. Electron Spectrosc. Relat. Phenom. **97**, (1998) (special issue on photoelectron spectroscopy of transients).
[3] J. Stöhr, *NEXAFS Spectroscopy* (Springer, New York, 1992).
[4] A. P. Hitchcock, Phys. Scr. **T31**, 159 (1990).
[5] A. P. Hitchcock and D. C. Mancini, J. Electron Spectrosc. Relat. Phenom. **67**, 1 (1994). (Updates to Aug-98 are available upon request.)
[6] R. W. Kirk and P. L. Timms, Chem. Commun. **1**, 18 (1967).
[7] O. Gropen and E. Wisløff-Nilssen, J. Mol. Struct. **32**, 21 (1976).
[8] E. F. Pearson and R. V. McCormick, J. Chem. Phys. **58**, 1619 (1973).

[9] H. W. Kroto, R. J. Suffolk, and N. P. C. Westwood, Chem. Phys. Lett. **22**, 495 (1973).
[10] T. P. Fehlner and D. W. Turner, J. Am. Chem. Soc. **95**, 7175 (1973).
[11] R. L. Sams and A. G. Maki, J. Mol. Struct. **26**, 107 (1975).
[12] A. M. Mebel, D. G. Musaev, and K. Morokuma, J. Phys. Chem. **97**, 7543 (1993).
[13] E. P. F. Lee, D. Wang, F. Chau, and X. Song, J. Electron Spectrosc. Relat. Phenom. **97**, 49 (1998).
[14] F. Grein, J. Mol. Spectrosc. **115**, 47 (1986).
[15] M. T. Nguyen and P. Reulle, J. Chem. Soc., Faraday Trans. 2 **80**, 1225 (1984).
[16] E. R. Talaty, Y. Huang, and M. E. Zandler, J. Am. Chem. Soc. **113**, 779 (1991).
[17] M. T. Nguyen, L. G. Vanquickenborne, M. Sana, and G. Leroy, J. Phys. Chem. **97**, 5224 (1993).
[18] R. J. Suffolk, T. A. Cooper, E. Pantelides, J. D. Watts, and H. W. Kroto, J. Chem. Soc. Dalton Trans. **1988**, 2041.
[19] W. P. Sholette and R. F. Porter, J. Phys. Chem. **67**, 117 (1963).
[20] E. R. Lory and R. F. Porter, J. Am. Chem. Soc. **93**, 6302 (1971).
[21] Y. Kawashima, K. Kawaguchi, and E. Hirota, Chem. Phys. Lett. **131**, 205 (1986).
[22] Y. Kawashima, Y. Endo, K. Kawaguchi, and E. Hirota, Chem. Phys. Lett. **135**, 441 (1987).
[23] Y. Kawashima, Y. Endo, and E. Hirota, J. Mol. Spectrosc. **133**, 116 (1989).
[24] C. Thomson and B. J. Wishart, Theor. Chim. Acta **35**, 267 (1974).
[25] M. Page, J. Phys. Chem. **93**, 3639 (1989).
[26] M. T. Nguyen, P. J. Groarke, and T. Ha, Mol. Phys. **75**, 1105 (1992).
[27] M. Sana, G. Leroy, and C. Wilante, Organometallics **11**, 781 (1992).
[28] J. Tyrell, J. Phys. Chem. **83**, 2906 (1979).
[29] P. Botschwina, Chem. Phys. **28**, 231 (1978).
[30] M. Alberti, A. Solé, and A. Aguilar, J. Chem. Soc., Faraday Trans. **87**, 37 (1991).
[31] M. Alberti, R. Sayós, A. Solé, and A. Aguilar, J. Chem. Soc., Faraday Trans. **87**, 1057 (1991).
[32] G. J. Mains, J. Phys. Chem. **95**, 5089 (1991).
[33] C. H. Chang, R. F. Porter, and S. H. Bauer, Inorg. Chem. **8**, 1689 (1969).
[34] B. S. Ault, Chem. Phys. Lett. **157**, 547 (1989).
[35] R. N. S. Sodhi and C. E. Brion, J. Electron Spectrosc. Relat. Phenom. **34**, 363 (1984).
[36] N. Kosugi, Theor. Chim. Acta **72**, 149 (1987).
[37] N. Kosugi and H. Kuroda, Chem. Phys. Lett. **74**, 490 (1980).
[38] S. Huzinaga, J. Andzelm, M. Klobokowski, E. Radzio-Andzelm, Y. Sasaki, and H. Tatewaki, *Gaussian Basis Sets for Molecular Calculations* (Amsterdam, Elsevier, 1984).
[39] S. G. Urquhart, Ph.D. thesis, McMaster University, 1997.
[40] W. H. E. Schwartz, Chem. Phys. **11**, 217 (1975).
[41] M. W. Chase, *NIST-JANAF Thermochemical Tables*, 4th ed., J. Phys. Chem. Ref. Data **9**, 14 (1985).
[42] *Inorganic Sulfur Chemistry*, edited by G. Nickless (Elsevier, New York, 1968).
[43] R. K. Iler, *The Chemistry of Silica: Solubility, Polymerization, Colloid, and Surface Properties and Biochemistry of Silica* (Wiley, New York, 1979).
[44] E. N. Aleksandrov, V. I. Vedeneev, I. V. Dubrovina, O. Y. Kalekin, S. N. Kozlov, V. V. Prakh, and K. G. Scherbina, Bull. Acad. Sci. USSR Chem. Sci. **37**, 1964 (1988).
[45] N. L. Garland, C. T. Stanton, and H. H. Nelson, J. Chem. Phys. **95**, 2511 (1991).
[46] W. V. F. Brooks, C. C. Costain, and R. F. Porter, J. Chem. Phys. **47**, 4186 (1967).